EnKF assimilation of simulated spaceborne Doppler observations of vertical velocity: impact on the simulation of a supercell thunderstorm and implications for model-based retrievals

W. E. Lewis, G. J. Tripoli

Advances in Geosciences, 7, 343–348, 2006
SRef-ID: 1680-7359/adgeo/2006-7-343
European Geosciences Union

Advances in Geosciences

EnKF assimilation of simulated spaceborne Doppler observations of vertical velocity: impact on the simulation of a supercell thunderstorm and implications for model-based retrievals

W. E. Lewis and G. J. Tripoli

Department of Atmospheric and Oceanic Sciences, University of Wisconsin, Madison, Wisconsin, USA

Received: 31 October 2005 – Revised: 3 December 2005 – Accepted: 6 December 2005 – Published: 15 June 2006

Abstract. Recently, a number of investigations have been made that point to the robust effectiveness of the Ensemble Kalman Filter (EnKF) in convective-scale data assimilation. These studies have focused on the assimilation of ground-based Doppler radar observations (i.e. radial velocity and reflectivity). The present study differs from these investigations in two important ways. First, in anticipation of future satellite technology, the impact of assimilating spaceborne Doppler-retrieved vertical velocity is examined; second, the potential for the EnKF to provide an alternative to instrument-based microphysical retrievals is investigated.

It is shown that the RMS errors of the analyzed fields produced by assimilation of vertical velocity alone are in general better than those obtained in previous studies: in most cases assimilation of vertical velocity alone leads to analyses with small errors (e.g. $<1\,\mathrm{ms}^{-1}$ for velocity components) after only 3 or 4 assimilation cycles. The microphysical fields are notable exceptions, exhibiting lower errors when observations of reflectivity are assimilated together with observations of vertical velocity, likely a result of the closer relationship between reflectivity and the microphysical fields themselves. It is also shown that the spatial distribution of the error estimates improves (i.e. approaches the true errors) as more assimilation cycles are carried out, which could be a significant advantage of EnKF model-based retrievals.

1 Introduction

The Kalman filter (Kalman, 1960) has a rich history of success in a wide range of applications, but not until a computationally feasible Monte Carlo implementation was developed (Evensen, 1994) did its application to geophysical data assimilation become attractive. The Ensemble Kalman Filter (EnKF), so called because it relies on an ensemble of model forecasts to provide the requisite error statistics, has been applied to atmospheric data assimilation at scales ranging from the global (Houtekamer and Mitchell, 1998, hereafter HM) to the convective (Snyder and Zhang, 2003, hereafter SZ).

Future generations of satellites are anticipated to include Doppler capability[1], thus providing the possibility of heretofore unavailable observations of vertical velocity. Convective systems are by definition regions of enhanced vertical motion, and so an EnKF Observing System Simulation Experiment (OSSE) conducted on an idealized supercell thunderstorm, as in SZ, will provide an excellent opportunity for evaluating the potential impact of these data.

Dowell et al. (2004) broached the possibility of employing the EnKF in convective-scale wind and temperature retrieval, and here we extend their results to examine the potential of the EnKF in microphysical retrieval. In addition to forming a posterior estimate that comprises more information than the instrument-based retrieval alone, the EnKF would provide the ability to retrieve model fields which are not directly observable (such as rainfall), as well as provide superior spatiotemporal resolution and a straightforward means of quantifying retrieval error.

Section 1 sets out a brief review of the Ensemble Kalman Filter. Section 2 provides an overview of the experiment design and methodology. Section 3 presents the results of the experiments, and conclusions are presented in Sect. 4.

2 The Ensemble Kalman Filter

As mentioned above, the EnKF is a Monte Carlo implementation of the optimal linear filter developed by Kalman in 1960. Its implementation is illustrated by the following: letting $\boldsymbol{x}^f$ denote a column vector containing the model

Correspondence to: W. E. Lewis
(welewis@wisc.edu)

[1] Im, E. and Durden, S. L.: Spaceborne Atmospheric Radar Technology, Proceedings of the 2005 Earth-Sun System Technology Conference, http://www.esto.nasa.gov/conferences/estc2005/author.html, 2005

forecast, the analysis $\boldsymbol{x}^a$ obtained by assimilating a column vector, $\boldsymbol{y}$, of observations is

$$\boldsymbol{x}^a = \boldsymbol{x}^f + \mathbf{K}(\boldsymbol{y} - H(\boldsymbol{x}^f)). \quad (1)$$

H is a measurement operator, possibly nonlinear, which relates the model variables to the observations $\boldsymbol{y}$, and the matrix $\mathbf{K}$ is known as the Kalman gain. $\mathbf{K}$ provides the means for converting the discrepancy between model and observation at a particular point into a smooth increment applied to rest of the model domain. It is defined as

$$\mathbf{K} = \mathbf{P}\mathbf{H}^T(\mathbf{H}\mathbf{P}\mathbf{H}^T + \mathbf{R})^{-1}, \quad (2)$$

where $\mathbf{P}$ is the error covariance matrix of the model forecast $\boldsymbol{x}^f$ and $\mathbf{R}$ is the observation error covariance matrix. The matrix $\mathbf{P}$ has as many elements as the model state size squared (i.e. 10^{12} or 10^{14} elements, given a typical NWP model) and is thus impractical to compute directly. In addition, $\mathbf{H}$ will not in general be transposable if it is nonlinear. Fortunately these difficulties may be overcome if the covariances are computed from an ensemble of model forecasts as demonstrated by HM:

$$\mathbf{P}\mathbf{H}^T = \frac{1}{m-1}\sum_{i=1}^{m}(\boldsymbol{x}_i^f - \bar{\boldsymbol{x}}_i^f)(H(\boldsymbol{x}_i^f) - \overline{H(\boldsymbol{x}_i^f)})^T \quad (3)$$

$$\mathbf{H}\mathbf{P}\mathbf{H}^T = \frac{1}{m-1}\sum_{i=1}^{m}(H(\boldsymbol{x}_i^f) - \overline{H(\boldsymbol{x}_i^f)})(H(\boldsymbol{x}_i^f) - \overline{H(\boldsymbol{x}_i^f)})^T, \quad (4)$$

where the index i varies over the m ensemble members and the H indicates that the measurement operator may indeed be a nonlinear model operator.

Implementation of the EnKF thus requires that an initial ensemble of model states be defined, usually by perturbing a best-guess estimate of the initial state. Then, each ensemble member is integrated forward until observations become available, at which point Eqs. (3) and (4) are used to calculate the products $\mathbf{P}\mathbf{H}^T$ and $\mathbf{H}\mathbf{P}\mathbf{H}^T$. The Kalman gain $\mathbf{K}$ is then calculated from Eq. (2), and the analysis for each ensemble member may then be computed from Eq. (1). The result is an ensemble of m analyses which are then integrated forward to the next observation time. Since $\mathbf{K}$ is computed from an ensemble of model states (rather than propagated according to a linear model, as in the original Kalman filter), it is allowed to evolve in accord with the nonlinear dynamics of the NWP model. This "flow-dependence" is a very attractive feature of the EnKF, and will be addressed further in Sect. 3.

It is important to note that the EnKF (as well as the Kalman filter before it) is an algorithm for propagating the state probability density function (PDF) forward in time, assuming that the PDF is Gaussian and thus requiring only two moments – the mean and covariance – to completely specify it. In this framework, one can think of the m state vectors as random vectors drawn from the PDF, and the mean of these vectors as the best linear estimate (in the minimum variance sense) of the true PDF mean. The covariance matrix $\mathbf{P}$ is a measure of the spread of the ensemble members and thus a gauge for the quality of the estimate. The potential usefulness of the information contained in $\mathbf{P}$ will be discussed again in section 3. The extent to which $\mathbf{P}$ reflects the true error in the estimate depends in large part on the filter's optimality, and this in turn depends on a number of factors, among the most important of which is the well-recognized tendency of finite-sized ensembles to underestimate the forecast error covariance (Whittaker and Hamill, 2001, hereafter WH).

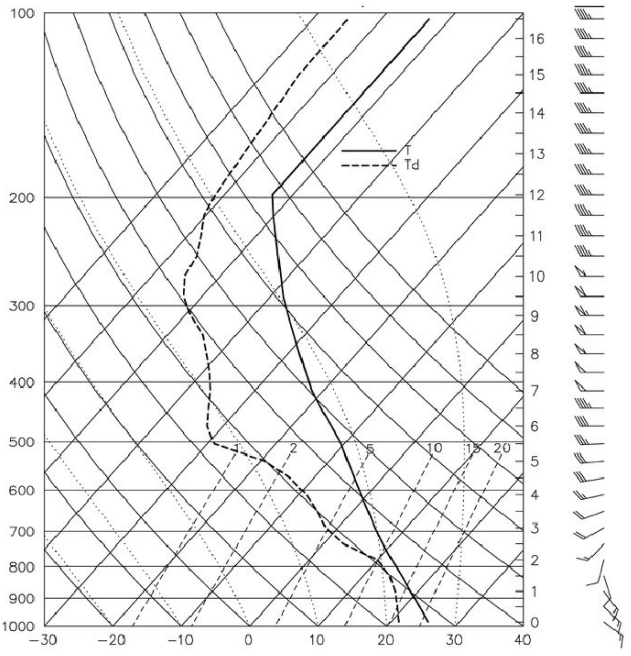

Fig. 1. Environmental sounding used to initialize the simulations. Temperature (°C) is denoted by the solid line and dewpoint (°C) by the dashed line. Wind vector magnitude is indicated by half barbs ($2.5\,\mathrm{m\,s^{-1}}$), full barbs ($5\,\mathrm{m\,s^{-1}}$) and flags ($25\,\mathrm{m\,s^{-1}}$) (after Snyder and Zhang, 2003).

3 Experiments

The experimental setup is largely the same as that employed in SZ and begins with the environmental sounding shown in Fig. 1. The University of Wisconsin Nonhydrostatic Modeling System (UW-NMS) (Tripoli, 1992) is initialized with this sounding on a domain employing 35 grid points in each spatial dimension. Grid spacing is 2 km in the horizontal, 500 m in the vertical and a time step of 10 s is used in integrating the model forward. Convection is initiated with a warm bubble at the surface center of the domain (nx=18, ny=18, nz=1) and $7\,\mathrm{ms^{-1}}$ is subtracted from the zonal wind component, u, in order to keep the storm within the computational domain.

In accordance with the above, a 100-minute "Truth" simulation (TR) is used to produce simulated observations of both vertical velocity, w, and equivalent reflectivity factor, Z_e (Smith, 1975). Since the minimum detectable signal (MDS) of the spaceborne Doppler instrument is anticipated to be $\sim$5 dBZ, observations of w and Z_e are saved only at those

Table 1. Description of Experiments.

Experiment	Field Assimilated	Observation Density	Observation Frequency
TR (TRUTH)	n/a	n/a	n/a
W2	w	2 km	$(5\,\text{min})^{-1}$
Z2	Z	2 km	$(5\,\text{min})^{-1}$
WZ2	w, Z	2 km	$(5\,\text{min})^{-1}$

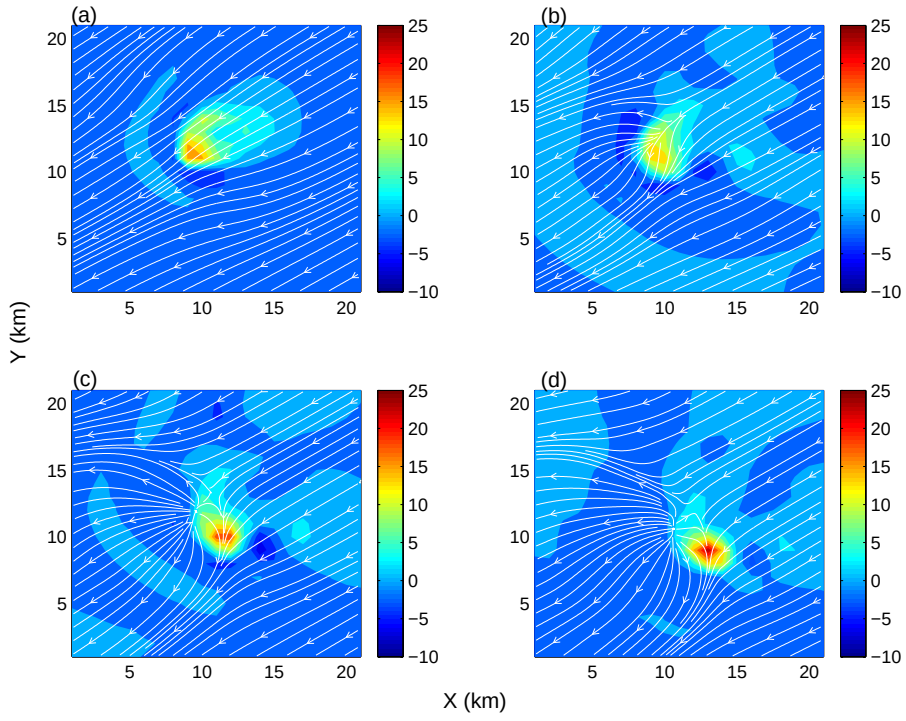

Fig. 2. Vertical velocity, w, at z=6 km (shaded) and surface streamlines at **(a)** t=30 min, **(b)** t=45 min, **(c)** t=60 min, and **(d)** t=75 min for the "Truth" simulation.

grid points where Z_e is greater than or equal to this threshold value.

Three assimilation experiments are conducted in which the observations as obtained above are assimilated using the EnKF. In the first experiment, denoted W2, observations of w are assimilated every five minutes beginning at t=25 min into the simulation (the point at which the number of observations exceeds several dozen) and is continued until t=100 min. Similarly, experiment Z2 involves the assimilation of Z_e, and experiment WZ2 involves the simulation of both w and Z_e. The experiments are summarized in Table 1.

Each of the assimilation experiments is begun by adding 40 separate realizations of uncorrelated, zero-mean Gaussian random noise to each gridpoint of the environmental sounding after it has been interpolated into model space and before the warm bubble is activated, thereby producing a 40-member ensemble. The standard deviation of the noise is $1\,\text{ms}^{-1}$ for the wind components and 1 K for the ice-liquid potential temperature, θ_{il}. The observation error covariance matrix, **R**, is assumed to be diagonal (i.e. observation errors are uncorrelated) and standard errors of $1\,\text{ms}^{-1}$ are assumed for the vertical velocity component, w, and a standard error of 5 dBZ is assumed for reflectivity.

Several additional details concerning the precise formulation of the EnKF algorithm need to be mentioned. First, a compact covariance localization scheme with local support (Gaspari and Cohn, 1999) is used to reduce the influence of distant, noisy covariance estimates owing to the finite-sized ensemble; in this case, only those elements of the covariance field lying within 6 km of the observation point are allowed to influence the analysis. This choice of localization radius is supported by consideration of the correlation and cross-correlation structure of the model fields as calculated from the ensemble (not shown). In a further effort to improve the optimality of the filter, both a square-root analysis scheme and a covariance inflation scheme as described in WH are employed. An inflation factor of 7% seems to produce the best results in conjunction with the chosen localization radius

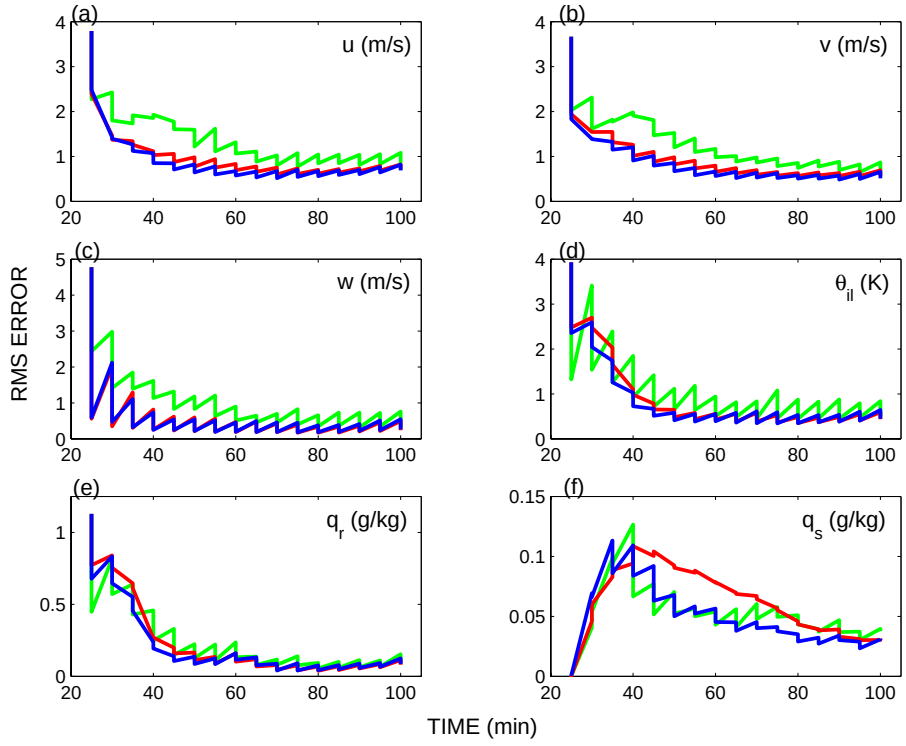

Fig. 3. RMS errors averaged over the domain where Z_e exceeds 5 dbz for **(a)** u, **(b)** v, **(c)** w, **(d)** θ_{il}, **(e)** q_r, and **(f)** q_s. Errors for u, v and w are in units of m s^{-1}. Errors for θ_{il} are in K. Errors for q_r and q_s are in g kg^{-1}. Red line indicates experiment W2, green line indicates Z2, and blue line indicates WZ2.

of 6 km. Finally, since **R** is assumed diagonal, observations are assimilated one at a time, allowing the analysis field resulting from the assimilation of one observation to become the forecast field for the next, and so on until all observations for a particular time period are assimilated (Anderson and Moore, 1979).

4 Results

The evolution of the "Truth" simulation can be seen in Fig. 2, which depicts vertical velocity (shaded) at z=6 km as well as streamlines of the horizontal wind at the lowest model level over the innermost 20 km of the model domain. At t=30 min (Fig. 2a) the storm has begun to split into right and left-moving cells, as two vertical velocity maxima are evident. By t=45 min (Fig. 2b) the right-moving cell has become dominant, as one would expect from the veering wind profile of the environmental sounding. The right-moving cell continues to intensify at t=60 min (Fig. 2c) and t=75 min (Fig. 2d), and an increasingly diffluent pattern is noted in the surface streamlines, indicative of the establishment of a well-defined rear-flanking downdraft.

In order to gauge the improvement of the analysis over time, the RMS errors of the ensemble mean of six model fields – u, v, w, θ_{il}, q_r , and q_s – are calculated. The errors are averaged over each gridpoint in the model domain where reflectivity equals or exceeds 5 dBZ and thus give a good indicator of filter performance. The errors at gridoints where Z_e<5 dBZ are very small, and, since they constitute a majority of the computational domain, their inclusion would serve to mask the robust reduction of error in the area of interest. Figures 3a, b, and c show the evolution of the RMS errors associated with the u, v, and w compnents of the wind, respectively, with experiment W2 depicted by the red line, experiment Z2 by the green line, and experiment WZ2 by the blue line.

Several trends are apparent. First, the largest impact occurs during the first few assimilation cycles. Second, the assimilation of reflectivity generally produces inferior results compared to the assimlation of vertical velocity, especially during the first 30 or 40 min of the assimilation. Tong and Xue (2005) noted similar behavior and attributed it to the evolution of the cross covariances associated with reflectivity. Since precipitation begins forming in the simulation only at t=20 min, and frozen precipitation only at t=30 min, it is reasoned that it takes some time for cross covariances between reflectivity and the other model fields to develop and become representative of the actual dynamics. Also of note is the magnitude of the errors. At t=40 min, the errors for u and v have been reduced to $\sim$1 ms^{-1} and the errors for w to $\sim$0.5 ms^{-1}. RMS errors this low are not achieved at any point during the 100 min simulation carried out by SZ. This improvement is attributed to the intrinsic value of vertical velocity as an observed field relative to observations

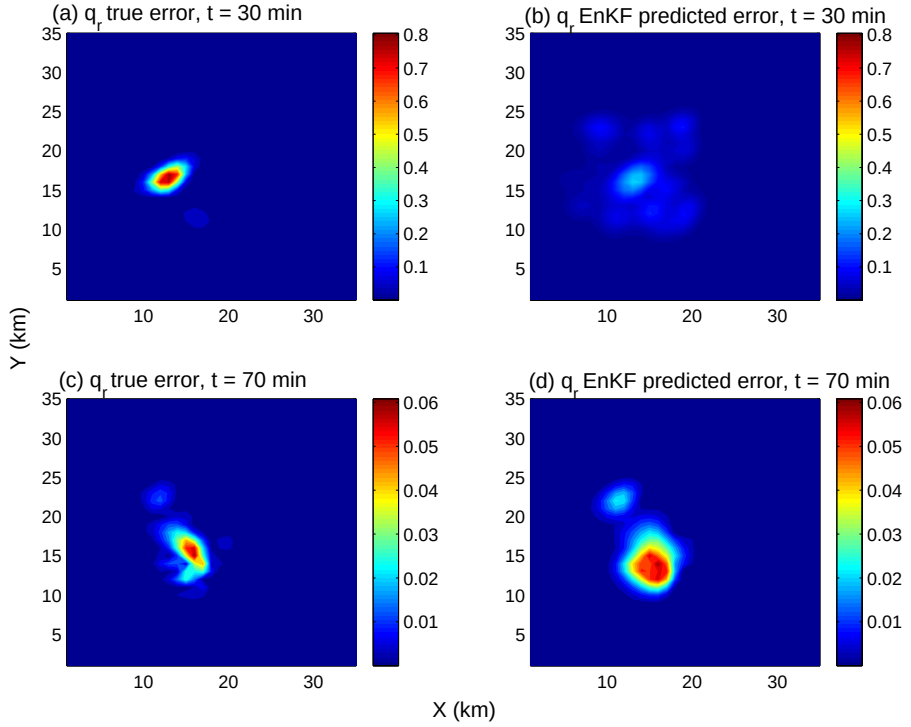

Fig. 4. Comparison of true and predicted errors in g kg^{-1} for q_r at the lowest model level. True errors at t=30 min and t=75 min are shown in **(a)** and **(c)** respectively, and predicted errors for t=30 min and t=75 min are shown in **(b)** and **(d)** respectively. Note the change in contour level between the two times.

of the horizontal wind, especially in cloud-resolving simulations such as the ones here. Not only do vertical velocity observations indicate the location of important features such as up- and downdrafts, they also provide immediate insight into the divergent part of the horizontal wind. Conversely, moving from observations of horizontal wind components to knowledge of the vertical motion field is much trickier (e.g. O'Brien, 1970).

The RMS errors for the ice-liquid potential temperature, θ_{il}, are shown in Fig. 3d, and the errors associated with the rainwater mixing ratio, q_r, and snow mixing ratio, q_s, are shown in Figs. 3e and f, respectively. The filter is less efficient in reducing the errors for these fields, with rainwater and especially snow revealing particularly refractory behavior. With regard to θ_{il}, the reason for the lag in error reduction vis-a-vis the velocity components is a somewhat more indirect dynamical coupling to the observations. For example, assimilation of w produces a rapid response in the analyzed w field, and a correspondingly rapid response (though smaller in magnitude) to the u and v fields since the horizontal and veritcal motion fields are related via continuity. The coupling of w to the θ_{il} field is more complex and involves diabatic processes, thus requiring a bit more time for the impact of the observations to translate to the analysis.

The microphysical fields reveal an interesting reversal of the relative impact of w and Z_e, namely that Z_e is as effective (rain) or superior (snow) to w in reducing the RMS errors. Here again, the reasoning is that reflectivity is more directly linked to the microphysical fields than is vertical velocity. Therefore, even though the cross-covariances associated with reflectivity are slow to develop with regard to the dynamical and thermodynamical fields, they develop somewhat more quickly with regard to the microphysical fields. It is interesting to note that over time, w becomes as effective as Z_e in reducing the microphysical errors, suggesting that once developed, the cross covariances associated with vertical velocity are more robust.

Finally, the potential role of the EnKF in performing model-based retrievals is explored. Given that bulk reduction of RMS error has been demonstrated here as well as in numerous other studies, the ability of the EnKF to produce spatial estimates of retrieval error provides a necessary complement. Shown in Fig. 4 are actual as well as predicted RMS errors for rainwater mixing ratio at the lowest model level. Figures 4a and b refer to true and predicted errors, respectively, at t=30 min, and Figs. 4c and d to true and predicted errors at t=75 min. At t=30 min, the predicted error field bears little resemblance to the actual error field, other than the identification of the locus of maximum error near x=12 km and y=17 km. Considerable improvement is noted by t=75 min. Indeed, the bimodel spatial distribution of the true error is captured nicely by the EnKF, although the magnitude of the error is overestimated by several hundredths of 1 g kg^{-1}, likely as a result of the simplistic covariance inflation scheme employed. Further improvement could likely be gained by using a more sophisticated (i.e. adpative) inflation

scheme and by increasing the size of the ensemble, but overall these results suggest that given a properly tuned filter, a reasonably accurate retrieval of the rain field can be achived after 50 min of assimilation. Similar results hold for the other dynamical, thermodynamical and microphysical fields (not shown).

5 Conclusions

It is shown that assimilation of vertical velocity with an EnKF produces RMS errors which are in general lower than those produced when only ground-based radial velocity is assimilated as in SZ. This result is anticipated given that convective systems, such as the supercell thunderstorm under consideration here, are characterized by their enhanced vertical motion fields. Accurate placement of up- and downdraft cores is crucial, as is properly resolving the divergent part of the horizontal wind. The EnKF, with its flow-dependent gain matrix, provides an effective means of accomplishing this latter task, as information contained in observations of w is spread to u, v and indeed to all other model fields in a dynamically consistent manner.

Given that future generations of satellites will include Doppler capability, the potential for producing better convective-scale forecasts certainly exists. However, several caveats must be stated. First, the observation density (2 km) and period (5 min) is greater than would initially be available from spaceborne Doppler radar. Second, more realistic results are to be anticipated from direct assimilation of vertical hydrometeor velocity as measured by radar (as opposed to the vertical component of the wind, as is done here). Further experiments which address these issues, as well as apply the methodology developed here to other convectively active systems such as tropical cyclones, are in progress.

Also encouraging is the potential for the EnKF framework to form a viable, perhaps eventually superior, alternative to traditional instrument-based retrieval. The EnKF allows retrieval of fields which are not directly observable and current generation NWP models provide spatiotemporal resolution which is greater than that of most instruments, meaning that retrievals would be available at virtually any place and time required. In addition, the EnKF provides a means of directly computing the error structure associated with the estimate, namely through the evaluation of the sample covariance of the ensemble. If the retrievals produced through EnKF assimilation are to become an alternative to instrument-based retrieval, however, more work will be necessary to understand the impact of various sources of filter suboptimality. Improved methods of ensemble initialization (Evensen, 2004) as well as rigorous studies of error dynamics are essential.

Acknowledgements. This research was supported by NASA grant NNG04GA36G. The authors wish to thank V. Homar for suggestions that improved the manuscript, as well as T. Hashino and S. Knuth for benefiicial discussions.

Edited by: V. Kotroni and K. Lagouvardos
Reviewed by: V. Homar

References

Anderson, B. D. O. and Moore, J. B.: Optimal Linear Filtering, Prentice Hall Inc., p. 143, 1979.

Dowell, D. C., Zhang, Z., Wicker, L. J., Snyder, C., and Crook, N. A.: Wind and Temperature Retrievals in the 17 May 1981 Arcadia, Oklahoma Supercell: Ensemble Kalman Filter Experiments, Mon. Wea. Rev., 132, 1982–2005, 2004.

Evensen, G.: Sequential data assimilation with a nonlinear quasi-geostrophic model using Monte Carlo methods to forecast error statistics, J. Geophys. Res., 99(C5), 10 143–10 162, 1994.

Evensen, G.: Sampling strategies and square root analysis schemes for the EnKF, Ocean Dyn., 54, 539–560, 2004.

Gaspari, G. and Cohn, S. E.: Construction of correlation functions in two and three dimensions, Q. J. R. Meteorol. Soc., 125, 723–757, 1999.

Houtekamer, P. L. and Mitchell, H. L.: Data assimilation using an ensemble Kalman filter technique, Mon. Wea. Rev., 126, 796–811, 1998.

Kalman, R. E.: A new approach to linear filtering and prediction problems. Transactions of the AMSE, J. Basic Engineering, 82D, 33–45, 1960.

O'Brien, J. J.: Alternative Solutions to the Classical Vertical Velocity Problem, J. Appl. Meteorol., 9, 197–203, 1970.

Smith Jr., P. L., Myers, C. G., and Orville, H. D.: Radar reflectivity factor calculations in numerical cloud models using bulk parameterizations of precipitation processes, J. Appl. Meteorol., 14, 1156–1165, 1975.

Snyder, C. and Zhang, F: Assimilation of Simulated Doppler Radar Observations with an Ensemble Kalman Filter, Mon. Wea. Rev., 131, 1663–1677, 2003.

Tong, M. and Xue, M.: Ensemble Kalman Filter Assimilation of Doppler Radar Data with a Compressible Nonhyrdostatic Model: OSS Experiments, Mon. Wea. Rev., 133, 1789–1807, 2005.

Tripoli, G. J.: A Nonhydrostatic Mesoscale Model Designed to Simulate Scale Interaction, Mon. Wea. Rev., 120, 1342–1359, 1992.

Whittaker, J. S. and Hamill, T. M.: Ensemble Data Assimilation without Perturbed Observations, Mon. Wea. Rev., 130, 1913–1924, 2001.